Environmental conditions and bio-optical signature of a coccolithophorid bloom in the Patagonian shelf

Carlos Alberto Eiras Garcia,[1] Virginia Maria Tavano Garcia,[1] Ana Inés Dogliotti,[2] Amábile Ferreira,[1] Silvia I. Romero,[3] Antonio Mannino,[4] Marcio S. Souza,[1] and Mauricio M. Mata[1]

Received 12 August 2010; revised 22 November 2010; accepted 29 December 2010; published 25 March 2011.

[1] In January 2008, a patch of high reflectance detected by ocean color satellite images was sampled during a cruise over the southern Argentinean continental shelf. High calcite concentrations (particulate inorganic carbon (PIC)) found at the patch were associated with dominance of the coccolithophorid *Emiliania huxleyi*. Relatively low chlorophyll concentrations (0.29 to 1.48 mg m^{-3}) were found, but both particulate attenuation (0.27 to 1.15 m^{-1}) and backscattering coefficients at 660 nm (0.003 to 0.042 m^{-1}) were noticeably high. Particulate inorganic to organic carbon (POC) ratio (PIC:POC) was highly variable (0.02 to 1.1), but mostly high, showing a significant correlation with particulate backscattering coefficient at 660 nm ($r = 0.83$, $p < 0.005$). The spectral dependency of the backscattering coefficient followed Gordon et al. (2009). Both the time evolution analyses of normalized water leaving radiance at 551 nm (*nLw551*) and the high PIC:POC ratios suggested an advanced stage of the coccolithophorid bloom, therefore with high detached coccoliths:cell ratios. Moreover, this was supported by a strong correlation between PIC and both particulate backscattering ($r = 0.81$, $p < 0.005$) and particulate beam attenuation coefficient ($r = 0.7$, $p < 0.05$). Remote sensing reflectance data were strongly related to particle backscattering and backscattering ratio, but not to absorption. NASA operational algorithms overestimated chlorophyll by a factor of ~2 and estimated PIC with a relatively high root-mean-square (RMS) error (RMS = 97.9 μg PIC L^{-1}). Better estimates of PIC values (RMS = 81.5 μg PIC L^{-1}) were achieved when we used the original PIC-specific backscattering coefficient (Balch et al., 2005).

Citation: Garcia, C. A. E., V. M. T. Garcia, A. I. Dogliotti, A. Ferreira, S. I. Romero, A. Mannino, M. S. Souza, and M. M. Mata (2011), Environmental conditions and bio-optical signature of a coccolithophorid bloom in the Patagonian shelf, *J. Geophys. Res.*, *116*, C03025, doi:10.1029/2010JC006595.

1. Introduction

[2] The biogeographical distribution pattern of coccolithophorids in the global ocean provides important ecological information due to their relevance on Earth's climate system. The main reason resides on these unicellular algae's ability to produce $CaCO_3$ scales (or plates) called coccoliths, which are initially attached to the living cells and then released into the water column. The detached coccoliths are then deposited on the ocean floor via fecal pellets and marine snow [*Roth et al.*, 1975] contributing to the carbon pumping system [*Balch et al.*, 2005, and references therein].

[3] The best environmental conditions for coccolithophorid growth are high incident solar radiation and strong stratification in the upper layer and blooms are normally associated with silicate depletion and other specific nutrient conditions [*Tyrrell and Merico*, 2004; *Iglesias-Rodríguez et al.*, 2002]. The depletion of silicate is typically due to a previous diatom bloom, favoring calcite-bearing organisms in the competition. For instance, when nitrate, phosphate and other nutrients are still abundant but dissolved silicate has been exhausted, coccolithophorids might outcompete diatoms [*Iglesias-Rodríguez et al.*, 2002; *Holligan et al.*, 1993]. Phosphate levels in the upper layer might also be low (high N:P ratios), since coccolithophorids are capable of uptaking dissolved organic phosphorus [*Tyrrell and Taylor*, 1995].

[4] *Boeckel et al.* [2006] have shown that the most common species (based on coccolith identification) encountered on surface sediments of the South Atlantic and Southern oceans is *Emiliania huxleyi* and that their relative abundance on the surface sediments of the continental margin off Argentina is among the highest (>80%).

[5] Early observations of ocean color images in the 80s have shown that one of the most extensive coccolithophorid blooms in the global ocean occurs at the Patagonian shelf

[1] Instituto de Oceanografia, Universidade Federal do Rio Grande, Rio Grande, Brazil.
[2] Instituto de Astronomía y Física del Espacio, Ciudad Universitaria, Buenos Aires, Argentina.
[3] Servicio de Hidrografía Naval, Buenos Aires, Argentina.
[4] NASA Goddard Space Flight Center, Greenbelt, Maryland, USA.

0148-0227/11/2010JC006595

region [*Brown and Yoder*, 1994; *Brown and Podestá*, 1997]. In true-color satellite images, areas of coccolithophorid blooms are generally recognized due to the light-scattering properties of algal cells and their associated coccoliths in the light spectrum, which may also induce errors in the determination of chlorophyll concentration from space using the operational empirical algorithms [*O'Reilly et al.*, 2000]. For such waters, a special algorithm was designed to recognize and estimate calcite concentration from space [*Gordon et al.*, 2001; *Balch et al.*, 2005].

[6] The magnitude of scattering by such blooms is not well understood worldwide due to several reasons. Coccolithophorid cells have a lower organic biomass compared to other monospecific blooms (e.g., diatoms) and generally their blooms are identified from space when coccoliths are in the process of detaching from the cells. The contribution of living calcifying cells and detached coccoliths in the backscattered light depends upon the stage of the bloom [*Balch et al.*, 1991]. The detached coccoliths also vary in size and shape, and the backscattering cross section and its spectral variation strongly depend upon the particle morphology [*Gordon and Du*, 2001]. More recently, *Gordon et al.* [2009] developed a model to deduce their scattering properties and also the influence of intact coccolithophorid cells on the apparent backscattering cross section of detached coccoliths.

[7] Due to the ecological importance of the Argentinean shelf waters and to its areal extension, several investigators have used a combination of satellite remote sensing and field observations to identify biogeochemical provinces [*Gonzalez-Silvera et al.*, 2004], to infer chlorophyll variability [*Garcia et al.*, 2004; *Rivas et al.*, 2006; *Romero et al.*, 2006] and to validate satellite-chlorophyll estimates [*Garcia et al.*, 2005; *Dogliotti et al.*, 2009] in the region. *Signorini et al.* [2006] used both chlorophyll [*O'Reilly et al.*, 2000] and calcite [*Gordon et al.*, 2001; *Balch et al.*, 2005] algorithms to show that high-reflectance coccolithophorid patches in the Patagonia shelf-break zone are most prominent in summer, after diatom and dinoflagellate blooms in spring [*Garcia et al.*, 2008].

[8] In the early days of January 2008, a high-reflectance patch, detected by satellite images, was sampled over the southern Argentinean continental shelf. This cruise was part of the Patagonia Experiment (PATEX) research project, which has the overall objective of characterizing the phytoplankton assemblages and primary production rates of the waters along the Argentinean shelf-break during spring and summer and their environmental constraints. Among methodologies used to assess these information were: measurements of physical properties (pressure, temperature, and salinity for computing density and water column stability); determination of main macronutrient levels (nitrate, phosphate, nitrite, silicate and ammonia) phytoplankton and pigments analyses; measurements of water-atmosphere CO_2 fluxes, aerosols and atmospheric biogenic gases (Dimethyl Sulphide (DMS)); measurements of bio-optical properties (hyperspectral remote sensing reflectance, light scattering, backscattering and absorption).

[9] In this article we report the original results and in situ observations carried out in a coccolithophorid bloom over the southern Patagonia continental shelf in early 2008. Such comprehensive field experiments and concurrent bio-optical properties measurements are quite rare in the Southern Hemisphere, and particularly in the southwestern Atlantic. The following section describes the data and methods used in this study. In section 3, we analyze the variability of the in situ bio-optical measurements, including chlorophyll-a concentration ([*chl*]), particulate and dissolved absorption coefficients (a_p and a_{CDOM}, respectively), particulate backscattering (b_{bp}), particulate beam attenuation coefficient (c_p), and also the remote sensing reflectance (R_{rs}) within the highly reflective patch observed in the satellite images. We also examine the variability of the particulate backscattering ratio (b_{bp}:b_p), which provides information on the marine particle composition and size distribution [*Boss et al.*, 2004; *Loisel et al.*, 2007; *Twardowski et al.*, 2001]. We carried out a Principal Component Analysis (PCA) and a correlation analysis between the first amplitude factor and the set of in situ bio-optical parameters to determine which are the main parameters that explain the observed variability in R_{rs}. Finally, concluding this study, we analyzed the performance of operational empirical algorithms currently used to derive chlorophyll and PIC concentration from satellite imagery.

2. Data and Methods

2.1. Cruise Details

[10] Prior to the cruise, we performed an analysis of true color composition and calcite MODIS-Aqua images of the Patagonian shelf to identify specific regions showing patches of probable coccolithophorid blooms. Images from 29 to 31 December 2007 were used to set up the sampling strategy for the early days of January 2008 (Figure 1). Sampling was conducted on board the Brazilian Navy RV *Ary Rongel* from early morning to late in the evening. A late arrival on the first day allowed only two stations to be visited on 4 January 2008. During the next day, only four stations were occupied because of bad weather conditions. Other twelve stations were carried out over the following 2 days. At the end of the cruise, three transects were performed between 4 and 7 January 2008, which allowed us to sample different water properties at 18 stations (Figure 1).

[11] A CTD-carousel SeaBird system was used to make casts in 17 of the 18 sampled stations. The number of CTD stations per transect was 7 (Section 1), 5 (Section 2) and 5 (Section 3). The CTD-carousel system was equipped with a CTD SeaBird 911 and a SBE32 carousel with sensors for measuring pressure, temperature, conductivity, Photosynthetic Available Radiation (*PAR*), stimulated chlorophyll fluorescence (WetLabs), dissolved oxygen (SeaBird) and beam transmittance at 660 nm (WetLabs®). The carousel comprised 12 Niskin bottles (5 L capacity) for sampling water at discrete depths for different measurements, including nutrients and chlorophyll concentration. In addition, samples from both surface and fluorescence peak depths were taken for chlorophyll-a concentration by High-Performance Liquid Chromatography (HPLC). Surface waters were sampled for light absorption by particulate (phytoplankton and detritus) and dissolved (Colored Dissolved Organic Matter (CDOM)) material.

[12] An optical frame was deployed using a 6 m long crane on the sunny side of ship's starboard side, away

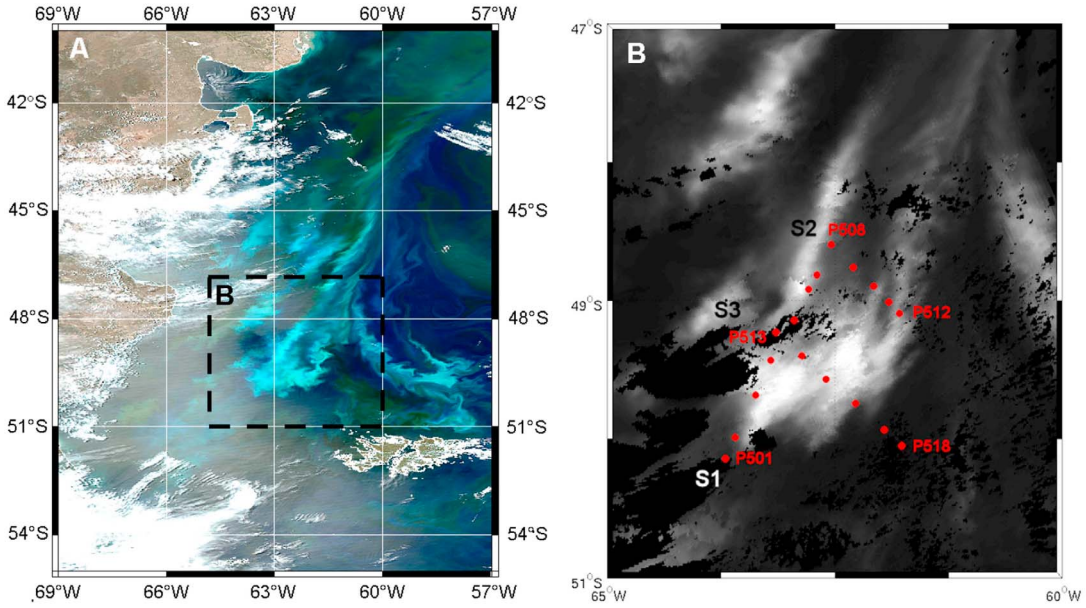

Figure 1. (a) MODIS quasi-true-color image on 31 December 2007 and (b) MODIS normalized water-leaving radiance at 551 nm composite image (3–8 January 2008) of the area sampled during the PATEX 5 cruise. The positions of the 18 in situ stations are indicated. Section 1 (S1) comprises stations P501 through P508, Section 2 (S2) comprises stations P508 through P512, and Section 3 (S3) comprises stations P513 through P518.

from the ship shadow. The following optical instruments were attached to the optical frame: backscattering meter at 530 and 660 nm (WetLabs) and hyperspectral radiometer (Satlantic Inc). The frame was lowered to 30–40 m deep to provide optical measurements in the upper water column. High-resolution optical data over the depth were achieved by a descending frame speed of about 20–30 cm s^{-1}.

2.2. In Situ Bio-optical Measurements

2.2.1. Chlorophyll-a Concentration

[13] Discrete samples for determination of pigment concentration were collected from the surface and selected depths based on the fluorescence profiles, provided by the CTD/Rosette system. The samples were filtered onto Whatman GF/F filters and kept frozen in liquid nitrogen until analyzed. Chlorophyll-a concentration, [*chl*], was determined by High-Performance Liquid Chromatography (HPLC) technique [*Mendes et al.*, 2007] only at surface and fluorescence peak depth. Chlorophyll-a concentration was also determined by using a Turner Designs TD-700 fluorometer [*Welschmeyer*, 1994] at several discrete depths. However, all chlorophyll-a concentrations used in this work are derived from HPLC method, except the vertical distributions of chlorophyll concentration (shown in Figure 6).

2.2.2. Phytoplankton Counting and Biovolume Estimation

[14] For phytoplankton identification, counting and sizing, water samples were preserved in amber glass flasks (~250 mL) with 2% alkaline Lugol's iodine solution. Phytoplankton cells in settling chambers (10 to 50 mL) were observed on a Zeiss Axiovert 135 inverted microscope [*Sournia*, 1978]. A scanning electron microscope (SEM) was used for identification of coccolithophorids. The cells concentration (expressed in 10^6 cells L^{-1}) was converted into biovolume, taking into account linear dimensions from captured images by a camera (Spot Insight QE) attached to the microscope. At least 30 specimens were randomly chosen for metrics of each species or major taxa and, then, biovolume was estimated using the most similar geometric shape [*Hillebrand et al.*, 1999].

2.2.3. Hyperspectral Reflectance

[15] Vertical profiles of downwelling spectral irradiance, E_d, and upwelling radiance, L_u, were measured using a hyperspectral ocean color radiometer (HyperOCR, Satlantic Inc.). Measurements were made over the spectral region 380–800 nm with a spectral resolution of 3.3 nm. Each band has a full-width-half-maximum (FWHM) bandpass of 10 nm. Internal tilt sensors quantified the vertical orientation of the profiler as it fell through the water column and were used as a quality control flag during data processing. A correction for the immersion effect was applied to radiometric measurements through the instrument's calibration coefficients (Satlantic, 2002). Profiles were corrected for pressure transducer depth offset relative to each sensor. No correction for sensor self-shading was applied. Initial data processing was done using ProSoft v. 7.7.11 software, also developed and distributed by Satlantic Inc. Dark offsets and manufacturer's radiometric calibration were applied to the raw data. Then, the optical data were binned to every 0.1 m. For the first 10 m, the instrument's median tilt angle was calculated for each profile and data with tilt angles greater than one standard deviation were discarded. After that, each profile was visually analyzed and the depth intervals for the surface extrapolation were

selected, generally starting at 2 m in order to avoid wave focusing. The spectral diffuse attenuation coefficients of downwelling irradiance, $K_d(\lambda)$, and upwelling radiance, $K_L(\lambda)$, were calculated as the local slope of a least squares regression of the log-transformed E_d and L_u, respectively, within the selected depth interval. Using these coefficients, the upwelling radiance values were propagated to just below the water surface, $E_d(0^-, \lambda)$ and $L_u(0^-, \lambda)$, by fitting an exponential function to the data. The remote sensing reflectance just above the sea surface, $R_{rs}(\lambda)$, was then calculated using the following equation:

$$R_{rs}(\lambda) = \frac{0.54 L_u(0^-, \lambda)}{1.04 E_d(0^-, \lambda)}$$

The coefficients 0.54 and 1.04 are the transfer coefficients of the air-sea interface for L_u and E_d, respectively [*Austin*, 1974].

2.2.4. Backscattering Coefficient

[16] Backscattering measurements were obtained with an ECO BB2F (WetLabs®, Philomath, Oregon) at two wavelengths (532 and 660 nm) within the visible range. The ECO BB2F measures the volume scattering function at a nominal angle of 117°, $\beta(117°)$. The particle volume scattering function, $\beta_p(117°)$, is then calculated by subtracting the volume scattering of water [*Morel*, 1974] from $\beta(117°)$. Finally, the particulate backscattering coefficient, $b_{bp}(\lambda)$, is estimated by assuming a constant proportionality between $\beta_p(117°)$ and b_{bp} [$=2\pi$ (1.1) $\beta_p(117°)$] [*Boss and Pegau*, 2001]. Raw data were processed using ProSoft software (Satlantic) and then calibrated using the ECO BB2F calibration files provided by WetLabs®.

2.2.5. Beam Attenuation Coefficient

[17] A *WetLabs C-star*® transmissometer attached to the CTD/carousel system was used to measure light attenuation at 660 nm. According to the C-Star calibration protocol, after calibrating and processing the raw data, the transmissometer provides the beam attenuation coefficients corrected for the attenuation by pure seawater, $c - c_w$. In the open ocean, absorption of dissolved material has little influence on the attenuation coefficient at 660 nm [*Pak et al.*, 1988], therefore the measured attenuation coefficient can be attributed only to particles (c_p). In order to eliminate uncertainties related to calibration, the c_p value of 0.12 m^{-1} measured in deep (particle-free) waters (~1,000 m) and far away from the sea bottom was measured and subtracted from each beam attenuation value in all profiles.

2.2.6. Spectral Absorption Coefficient

[18] Discrete samples from the surface, collected at all 18 stations, were filtered onto 25 mm Whatman GF/F filters for measurements of light absorption by particulate material and colored dissolved organic matter (CDOM). The optical density values of the particulate material retained in the filters were determined using a dual beam scanning spectrophotometer (Cary Model 1E). Values corresponding to detritus were determined after pigment bleaching with pure methanol [*Mitchell et al.*, 2000]. Absorption coefficients (m^{-1}) for total particulate matter, $a_p(\lambda)$, and for detritus, $a_{det}(\lambda)$, were then calculated by converting optical density at each wavelength to natural log, normalizing by the filtered volume and applying a Beta factor [*Ferreira et al.*, 2009], which corrects for the effect of concentrating particles on filters. The spectral absorption coefficients for phytoplankton, $a_{ph}(\lambda)$, were computed as the difference between $a_p(\lambda)$ and $a_{det}(\lambda)$ estimates. Filtrates from the particulate absorption sample filters (Whatman GF/F) were collected in clean borosilicate bottles that were previously treated according to *Mitchell et al.* [2000]. Fresh Mili-Q water was used to zero the instrument and the spectral absorbance of the filtered water was measured against air in a 10 cm quartz cuvette between 300 and 750 nm. Optical density values were converted into CDOM absorption coefficients, $a_{CDOM}(\lambda)$ (m^{-1}).

2.2.7. Particulate Organic and Inorganic Carbon

[19] Discrete water samples from surface and depth of the fluorescence peak were analyzed for particulate organic and inorganic carbon. Particles for particulate carbon (*PC*), nitrogen (*PN*) and particulate organic carbon (POC) were collected onto precombusted (450°C for 4–6 h) 25 or 47 mm Whatman GF/F glass fiber filters and stored frozen (−20°C). Prior to analysis, the filters were dried for ~48 h in a drying oven at 45–50°C. POC samples were placed overnight (24 h) in a sealed desiccator saturated with hydrochloric acid fumes (12M HCl) to remove inorganic carbon from samples [*Hedges and Stern*, 1984]. Acidified filters were dried again as described previously. Sample filters were packed into tin foil sheets for analysis. POC, *PC* and *PN* were measured with a vario MICRO cube CHNS elemental analyzer (Elementar Americas, Mt. Laurel, NJ). Sulfanilamide, the manufacturer recommended calibration standard, was run daily (prior to sample analysis and interspersed between samples) to compute the daily factor, the variation between the daily instrument response relative to the factory calibration, in order to apply the appropriate calibration factor. Sample carbon and nitrogen were corrected for carbon and nitrogen content measured for triplicate tin foil sheet blanks. Particulate inorganic carbon (PIC) was computed as the difference between *PC* (filters not acidified) and POC (acidified filters). Analytical error for duplicate POC measurements averaged 12.2% for these samples. A reference standard for carbon, Buffalo River Sediment (BRS) NIST reference material NIST RM 8704; 3.348 ± 0.016% C), was analyzed three times per day to confirm the performance of the standards and calibration curve. Our analysis of the BRS NIST RM yielded results equivalent to the NIST values (3.348 ± 0.062%C; n = 25; analyzed on nine separate days).

2.3. Satellite Data

[20] Satellite ocean color data used here were derived from MODIS, available at the Ocean Color Web site (http://oceancolor.gsfc.nasa.gov). Cloudy skies dominated over the 4 day sampling period, so in situ AOP and IOP data were acquired under overcast conditions. Daily visualization of satellite images was performed during the entire period of the cruise. However, due to cloud conditions during the cruise, the bloom patch could only be distinguished in the image of 5 January. Because coccolithophorid blooms (and detached coccoliths) strongly backscatters green light [*Gordon and Balch*, 1999], we decided to examine the time evolution of normalized water leaving radiance at 551 nm, *nLw551*, from 28 December 2007 to 12 January 2008.

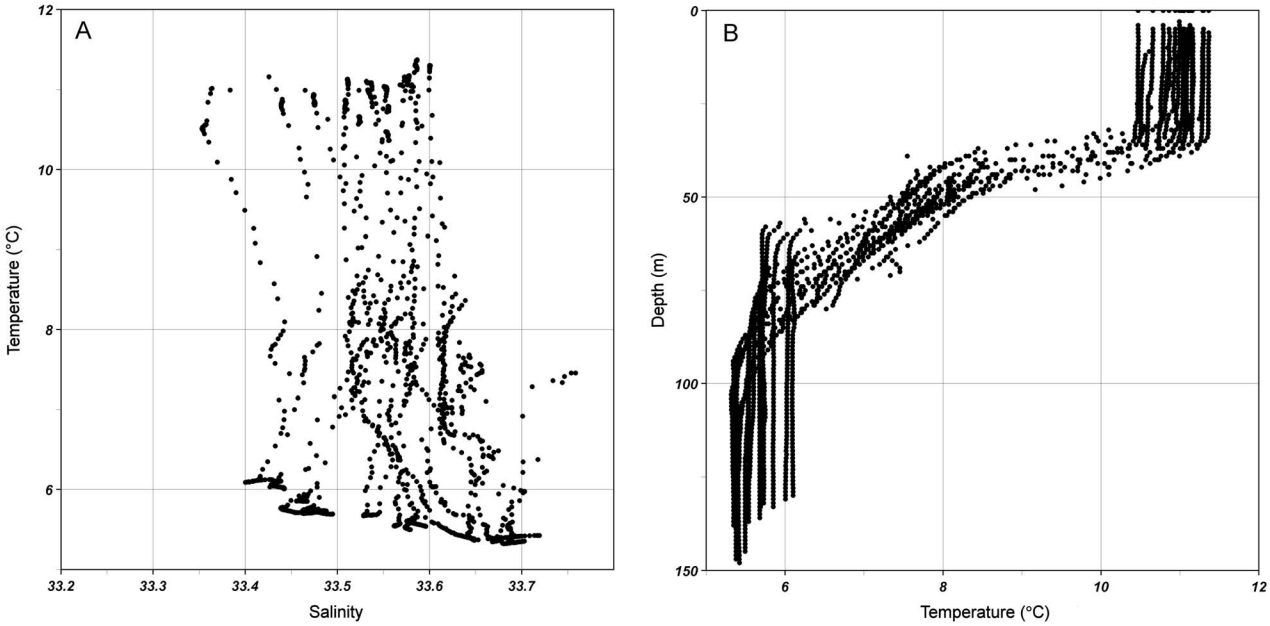

Figure 2. (a) $T - S$ diagram (temperature and salinity) from all stations sampled during the PATEX 5 cruise. (b) Temperature vertical profiles at the same stations. Mixed layer depths are limited to ~30–35 m.

We noticed that both bloom size and *nLw551* values had decreased during this period, suggesting that the timing of the in situ sampling corresponded to an advanced stage of the coccolithophorid bloom, with high liths:cell ratios. No comparison between satellite and in situ measured *nLw* or [*chl*], the well-known matchup procedure, was made due to lack of cloud-free images.

2.4. Statistical Analysis

[21] A Principal Component Analysis (PCA) was applied over the whole $R_{rs}(\lambda)$ spectra data set to extract the R_{rs} variance structure [*Lubac and Loisel*, 2007], assessing the variability modes of $R_{rs}(\lambda)$. As a previous step, the mean spectrum was subtracted from each single spectrum to produce a centered data set. Then, in order to examine the $R_{rs}(\lambda)$ variability and the bio-optical parameters most likely affecting it, a correlation analysis was performed between the first amplitude factor and several in situ bio-optical parameters such as [*chl*], backscattering ratio, scattering and absorption coefficients, PIC and POC concentration and coccolithophorid cell concentration (number and percentage). Further details on the phytoplankton community (see section 2.2.2) are presented by *Souza et al.* [2011].

3. Results

3.1. The Physical Environment

[22] During the sampling period, surface salinity and temperature varied from 33.3 to 33.6 and from 10.2 to 10.7°C, respectively. A $T - S$ diagram of all stations is seen in Figure 2a, where a salinity (S) gradient (33.3 to 33.6) was observed from south (lower values) to north (higher values) and from east (lower values) to west (higher values). Diluted waters, probably from Magellan Strait area, present $S < 33.3$. A shallow mixed layer depth of about 35 m was found (Figure 2b) at all stations. C. B. Marin (Water mass, thermohaline structure and nutrient levels in the Patagonian shelf-break waters during the Patagonian Experiment (PATEX), manuscript in preparation, 2011) has shown that low nutrients levels (nitrate ~2 μM and silicate ~0.4 μM) in the mixed layer and high values (nitrates ~15 μM, silicates ~2 μM) below the thermocline are caused by both phytoplankton consumption in the upper layer and sharp density vertical gradients. Overall, vertical dissolved oxygen and fluorescence were not closely related (not shown), as opposed to the positive relationship found between oxygen and [*chl*] during a spring bloom (October) of diatoms in the shelf-break region [*Garcia et al.*, 2008].

3.2. Phytoplankton Microscope Data

[23] The surface concentration of *E. huxleyi* cells varied between 0.05 and 11 × 10^6 cell L^{-1} at the cruise stations. The percentage of *Emiliania huxleyi* cells in the phytoplankton assemblage varied from 1.5% (St. P517) up to 93.7% (St. P503). In terms of biovolume data, *E. huxleyi* represented between 1.2 and 94.8% of total biovolume. Smaller coccolithophorid contributions (1 to 3.3%) were detected at stations P513, P517 and P518, where the phytoplankton was mainly represented by dinoflagellates (St. P513) and cryptophytes/dinoflagellates (stations P517 and P518). Regarding other coccolithophorid species, larger cells (10–20 μm, probably *Coccolithus pelagicus*) were detected but they were very scarce and only significant at St. P503 (0.05 × 10^5 cell L^{-1}) and St. P513 (0.13 × 10^5 cell L^{-1}). Diatoms were important mainly at station P512 (>50% biovolume), while dinoflagellates showed a considerable contribution at most stations, followed by the haptophyte *Phaeocystis antarctica* [*Souza et al.*, 2011].

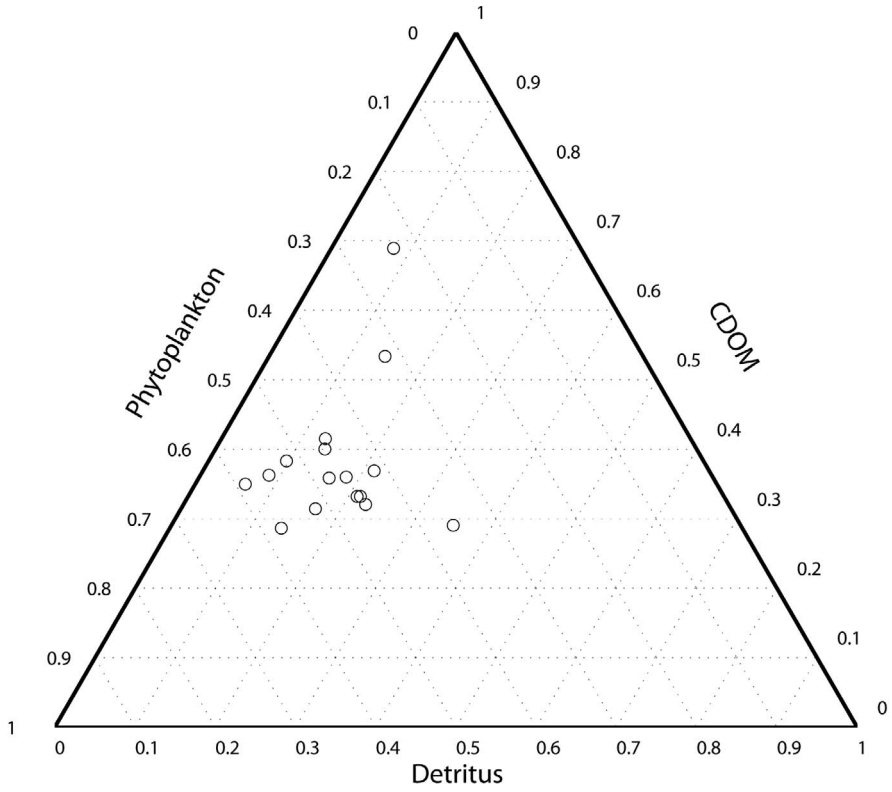

Figure 3. Ternary plot illustrating the relative contribution of CDOM, phytoplankton, and detritus to light absorption at 440 nm for all surface samples. The relative contribution of a component to total absorption can be read on the corresponding axis.

[24] The massive dominance of *E. huxleyi* at St. P503 through P506 and St. P514 and P515 was probably associated with relatively high concentration of detached coccoliths. For instance, *Balch et al.* [2000] found a ratio of approximately 5 to 6 detached coccoliths to whole coccolithophorid cells in the Arabian Sea.

3.3. Surface Distribution of Bio-optical Properties

[25] The surface bio-optical parameters measured over the sampled region were highly variable and their statistical parameters are summarized in Table 1. [*chl*] ranged between 0.29 (St. P504) and 1.48 mg m^{-3} (St. P512), with a mean concentration of 0.57 mg m^{-3}. Absorption of the particulate material, $a_p(440)$, varied between 0.073 and 0.193 m^{-1}, and the mean relative contribution of phytoplankton, $a_{ph}(440)$, to the particulate absorption, $a_p(440)$, was 0.73, with the lowest value at St. P514 (0.48), indicating that the phytoplankton dominated the particulate absorption (Figure 3). Moreover, a significant linear relationship between $a_{ph}(440)$ and [*chl*] was found (r = 0.70), and when the absorption values at 676 nm (values not shown) were considered, the relationship improved (r = 0.84). Linear fittings provided the best statistical results between [*chl*] and phytoplankton absorption at both wavelengths and the coefficients derived from the least squares method are provided in Table 2. The specific phytoplankton absorption coefficients at 440 nm, (i.e., $a_{ph}(440)/[chl]$, $a^*_{ph}(440)$), presented relative high values (mean of 0.168, std of 0.047), compared to global tendencies. Our $a_{ph}(440)$ values as a function of [*chl*] are higher than the mean relationship from *Bricaud et al.* [1995] by a mean factor of 3. Moreover, when our data are compared to *Bricaud et al.*'s [2004] equation, which were exclusively derived between HPLC [*chl*] and $a_{ph}(440)$, our coefficients are still twofold higher. The relatively higher $a^*_{ph}(\lambda)$ coefficients found in the Patagonian region have already been discussed by *Ferreira et al.* [2009] who attributed these differences to both an important influence of photoprotector accessory pigments and lower [*chl*] per cell, due to high incident light levels in the region.

Table 1. Statistical Parameters of Surface [*chl*] and Optical Properties for the 18 Stations, Sampled During the PATEX 5 Cruise[a]

	Range	Mean	Std. Dev	CV (%)
[*chl*]	0.29–1.48	0.565	0.284	50.2
$K_d(440)$	0.107–0.210	0.164	0.045	27.3
$a_p(440)$	0.073–0.193	0.12	0.033	27.3
$a_d(440)$	0.011–0.065	0.031	0.014	46.5
$a^*_{ph}(440)$	0.109–0.305	0.168	0.046	27.5
$a_{CDOM}(440)$	0.04–0.303	0.081	0.063	77.1
$c_p(660)$	0.27–1.15	0.67	0.328	49.0
$b_{bp}(660)$	0.0025–0.0419	0.0162	0.0121	74.4
$b_{bp}(660):b_p(660)$	0.0097–0.0376	0.023	0.0087	37.8

[a]Coefficient of variation (CV) corresponds to the ratio between standard deviation and mean value. $K_d(440)$ and b_{bp} were obtained at 16 stations.

Table 2. Coefficients of Correlation and Equations Derived Between Biogeochemical and Optical Parameters[a]

Correlated Parameters (x, y)	r	N	Equation
[*chl*], $a_{ph}(440)$	0.70	16	$a_{ph}(440) = 0.073\ [chl] + 0.042$
[*chl*], $a_{ph}(676)$	0.84	16	$a_{ph}(676) = 0.033\ [chl] + 0.0086$
[*chl*], $c_p(660)$	NS	16	-
[*chl*], $b_{bp}(660)$	NS	16	-
% *EH* cells, $b_{bp}(532)$	0.83	16	$b_{bp}(532) = 3.071 \times 10^{-4}$ % *EH* cells + 0.0054
% *EH* cells, $b_{bp}(660)$	0.83	16	$b_{bp}(660) = 3.208 \times 10^{-4}$ % *EH* cells + 0.0058
$b_{bp}(660)$, $c_p(660)$	0.94	16	$c_p(660) = 23.33\ b_{bp}(660) + 0.27$
$a_p(532)$, $b_{bp}(532)$	NS	16	-
$a_p(660)$, $b_{bp}(660)$	NS	16	-
$b_{bp}(532)$, $b_{bp}(660)$	0.99	16	$b_{bp}(660) = 1.0366\ b_{bp}(532) + 0.001$
[*chl*], POC	NS	10	-
POC, $a_p(440)$	NS	10	-
POC, $c_p(660)$	NS	10	-
POC, $b_{bp}(532)$	NS	10	-
PIC, $c_p(660)$	0.70	10	$c_p(660) = 2.4 \times 10^{-3}$ PIC + 0.39
PIC, $b_{bp}(532)$	0.81	10	$b_{bp}(532) = 1.1 \times 10^{-4}$ PIC + 0.004
PIC, $b_{bp}(660)$	0.81	10	$b_{bp}(660) = 1.1 \times 10^{-4}$ PIC + 0.005
PIC:POC, $b_{bp}(660)$	0.83	10	$b_{bp}(660) = 0.028$ PIC:POC + 0.0063
PIC:POC, $b_{bp}(660)/c_p(660)$	0.82	10	$b_{bp}(660)/c_p(660) = 0.015$ PIC:POC + 0.02

[a]All relationships are significant at 95% confidence level, except NS.

[26] The absorption due to particulate matter at 440 nm, where the particulate absorption is around its maximum, could only explain around half of the variability of the diffuse attenuation coefficient for downwelling irradiance, K_d, at the same wavelength ($r = 0.74$, $r^2 = 0.56$, N = 16, $p \ll 0.05$), suggesting that other factors (sun zenith angle, b/a ratio, and the respective proportion between molecular and total scattering coefficient) might control the light attenuation in the blue portion of the spectra besides the particulate absorption [*Loisel and Morel*, 1998]. The mean contribution of the dissolved material, $a_{CDOM}(440)$, to total absorption was 0.40. Wavelength-dependent (higher in the blue) scattering and absorption by coccoliths and coccolithophorids, respectively, might also be influencing the light attenuation [*Balch et al.*, 1991].

[27] Surface particulate backscattering coefficient, $b_{bp}(660)$, showed a large variability, ranging between 0.003 and 0.042 m^{-1} (coefficient of variation, CV = 74%), while the particulate attenuation coefficient at the same wavelength, $c_p(660)$, presented a smaller variation, ranging from 0.27 to 1.15 m^{-1} (CV = 49%). A strong linear relationship ($r^2 = 0.91$) between $c_p(660)$ and $b_{bp}(660)$ was found for surface waters (Figure 4). Note that St. P512 (dominated by diatoms) stands out in the regression with a relatively high $c_p(660)$ value (0.97 m^{-1}) and the highest [*chl*] value (1.48 mg m^{-3}), with a relatively small $b_{bp}(660)$ value (0.019 m^{-1}). If it is assumed that $a \ll b$, then $c \sim b$, and b_p/c is close to the backscattering probability (b_b/b). Figure 4 shows a regression line in which the inverse of slope (1/23.3287 ~ 0.0428) is very close to the modeled backscattering probability values at 660 nm [see *Gordon et al.*, 2009, Figure 11]. No significant correlations were found between $b_{bp}(660)$ (or $c_p(660)$) and a_{ph} (or [*chl*]), indicating that their variability is likely due to the presence of particles other than phytoplankton living cells, as confirmed in section 3.4. The backscattering ratios (b_{bp}:b_p) at 660 nm were relatively high, varying between 0.009 and 0.037 (CV = 40%), comparable to the values found in some coastal environments [*Twardowski et al.*, 2001; *Boss et al.*, 2004; *Chang et al.*, 2004; *Loisel et al.*, 2007] where high concentration of inorganic particles are present. The particulate backscattering coefficients at either 532 or 660 nm are well related ($r = 0.83$, $N = 16$, $p < 0.05$) to the percentage of *Emiliania huxleyi* cells in the phytoplankton assemblage composition (Table 2).

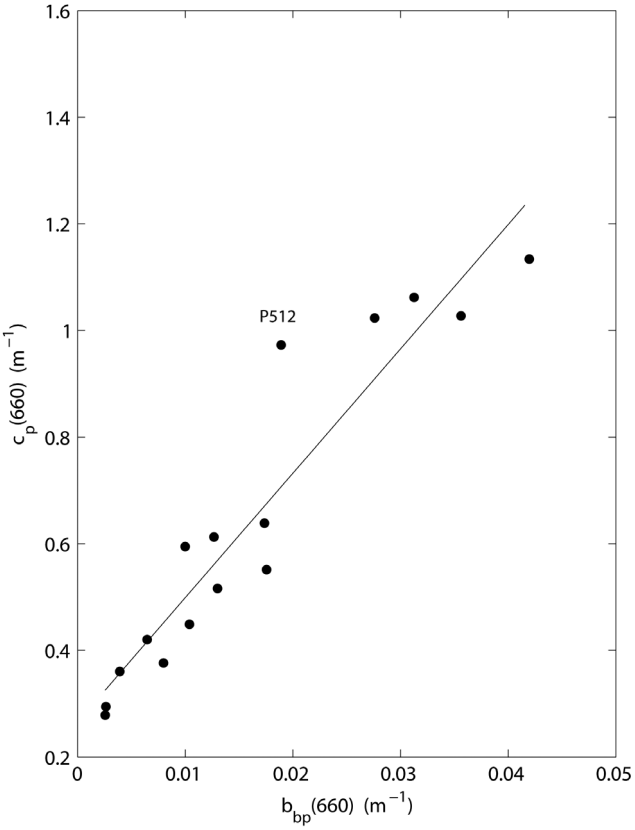

Figure 4. Beam attenuation at 660 nm versus backscattering at 660 nm for the 16 sampled stations during the PATEX 5 cruise. The correlation coefficient is $r = 0.88$ ($p < 0.0001$). The linear regression equation is $c_p(660) = 23.3287\ b_{bp}(660) + 0.266$. Station number P512 is indicated.

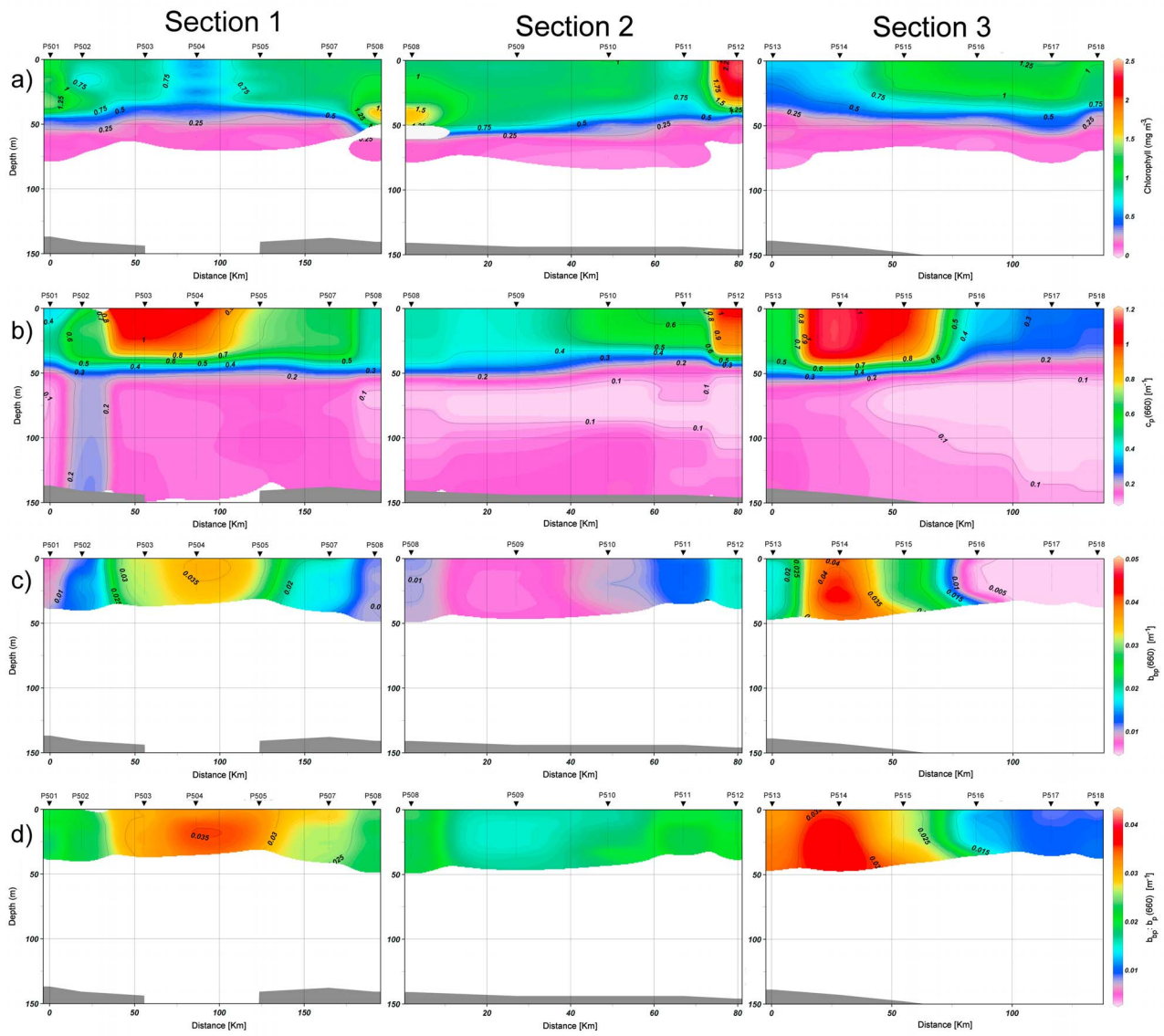

Figure 5. Water column distribution of (a) fluorometric [*chl*], (b) beam attenuation at 660 nm, (c) particulate backscattering at 660, and (d) backscattering ratio at 660 nm for Sections 1 (left), 2 (middle), and 3 (right). Station numbers are marked on top of each graph. See Figure 1 for location of the sections.

3.4. Vertical Distribution of Bio-optical Properties

[28] The vertical distributions of [*chl*], $c_p(660)$ and $b_{bp}(660)$ are presented in Figure 5 for Sections 1, 2 and 3 (see Figure 1 for location). A general strong gradient is observed around 35–40 m. In Section 1, which ran northward from St. P501 to P507, the upper 40 m were characterized by higher values in [*chl*], $c_p(660)$ and $b_{bp}(660)$ than in deeper waters (Figures 5a–5c, Section 1). Regarding the [*chl*] in the upper 40 m layer, stations P501 and P507 presented higher values (>1 mg m^{-3}) than the surrounding stations. St. P504 was characterized by lower [*chl*] (<0.5 mg m^{-3}), compared to the other stations, but relatively high $c_p(660)$ and $b_{bp}(660)$ values (~1 m^{-1} and >0.035 m^{-1}, respectively). The particulate backscattering ratio, b_{bp}:$b_p(660)$, distribution was similar to that of $b_{bp}(660)$, with higher values at station P504 (~0.03).

[29] In Section 2, [*chl*] was approximately constant (~1 mg m^{-3}) in the upper mixed layer (Figure 5a, Section 2), except at St. P508 where [*chl*] values were above 1.5 mg m^{-3} (at 50 m depth) and at St. P512 where [*chl*] reached 2.4 mg m^{-3} at the surface. The attenuation coefficient was nearly constant in the upper well mixed layer (~0.5 m^{-1}), except at St. P512 where higher values, around 1 m^{-1}, were found (Figure 5b, Section 2). Particle backscattering, $b_{bp}(660)$, in the upper layer showed some variations along this section, and relative higher values (~0.02 m^{-1}) were measured at St. P512. The backscattering ratio also followed the particulate backscattering coefficient distribution. Note that relatively high values (~0.02), compared to the surrounding stations, were found at stations P508 and P512, in good correspondence with high [*chl*].

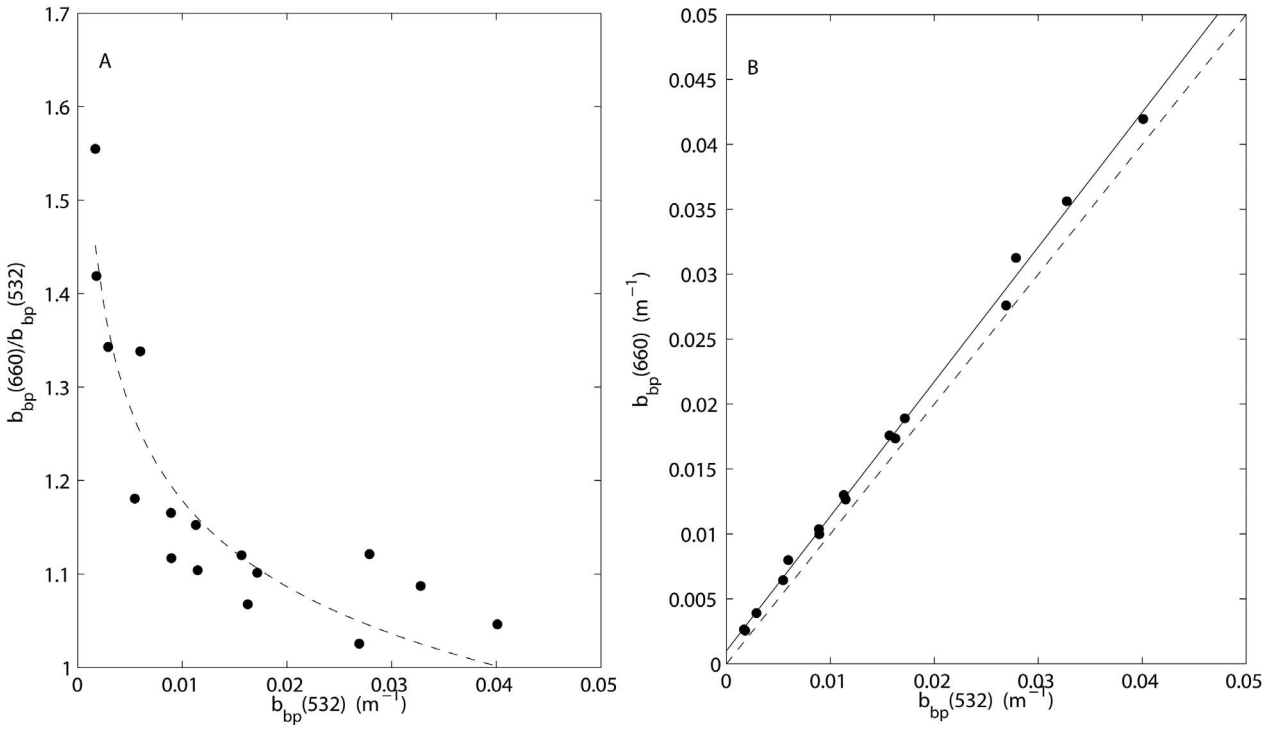

Figure 6. The relationships between (a) $b_{bp}(660)/b_{bp}(532)$ and $b_{bp}(532)$ and (b) $b_{bp}(660)$ and $b_{bp}(532)$. Observe that green-to-red particulate backscattering ratio is always greater than 1 but decreases toward unity at high $b_{bp}(532)$.

[30] In Section 3, [*chl*] in the upper mixed layer was unevenly distributed (Figure 5a, Section 3). Relatively high [*chl*] values (>1 mg m^{-3}) were found closer to sea surface at stations P515, P516 and P517. The highest mean [*chl*] in the mixed layer was measured at St. P517. Surface $c_p(660)$ values were lower at St. P518 and increased toward the middle of the section (>1 m^{-1} at St. P514). In this section, $b_{bp}(660)$ and b_{bp}:$b_p(660)$ also followed approximately the surface attenuation coefficient distribution with lower (~0.005 m^{-1} and ~0.04) and higher (~0.04 m^{-1} and 0.009) values than surrounding stations at stations P518 and P514, respectively.

3.5. Spectral Dependency of Optical Backscattering

[31] The spectral shape of total backscattering is usually determined by the following expression:

$$b_{bp}(\lambda) = b_{bp}(\lambda_0)\left(\frac{\lambda_0}{\lambda}\right)^{\gamma}$$

The exponent γ is the dimensionless parameter describing the spectral dependency of $b_{bp}(\lambda)$ to a reference wavelength λ_o. The exponent γ is sensitive to particle size distribution as well as to the relative contribution of organic to inorganic material, being the later more effective in backscattering light [*Loisel et al.*, 2007]. Values of γ varying from 0 to 2 have been widely used by inversion of ocean color spectra models [e.g., *Roesler and Perry*, 1995; *Garver and Siegel*, 1997]. The empirical model of *Morel* [1988], derived from in situ measurements in Case I waters, assumes that $b_{bp}(\lambda)$ depends on λ^{-1} indicating that stronger backscattering occurs at shorter wavelengths. *Gordon et al.* [2009] derived $b_b(\lambda)$ spectra from in-water radiance data during an *E. huxleyi* bloom in the English Channel, with a general pattern of maximum b_b in the blue decreasing toward the green reaching a minimum near 550–620 nm, and then increasing toward the red portion of the spectrum. The authors highlight that $b_b(\lambda)$ is not proportional to λ to some power (i.e., a "power law") over the entire visible spectrum.

[32] In our work, $b_{bp}(660)/b_{bp}(532)$ is inversely proportional to $b_{bp}(532)$ and it tends toward unity for high backscattering values (Figure 6a). This indicates that $b_{bp}(\lambda)$ tends to be independent on wavelength at very high backscattering values. It is worth noting that in our work, $b_{bp}(660)$ is always higher than $b_{bp}(532)$.

[33] Figure 6b shows the relationship between $b_{bp}(660)$ and $b_{bp}(532)$ where the slope is 1.0366. Assuming that a power law (equation above) holds in this portion of the spectrum (green to red), then the slope of the curve shown in Figure 6b can be interpreted as $(532/660)^{\gamma}$ which leads to $\gamma = -0.16$. This means that b_{bp} increases slightly from the green to the red portion of the visible spectrum, therefore close to what was observed by *Gordon et al.* [2009].

3.6. Relationship Between PIC, POC, and Inherent Optical Properties

[34] Mean particulate inorganic and organic carbon concentrations (PIC and POC, respectively) were calculated from surface and depths where b_b and c_p data were avail-

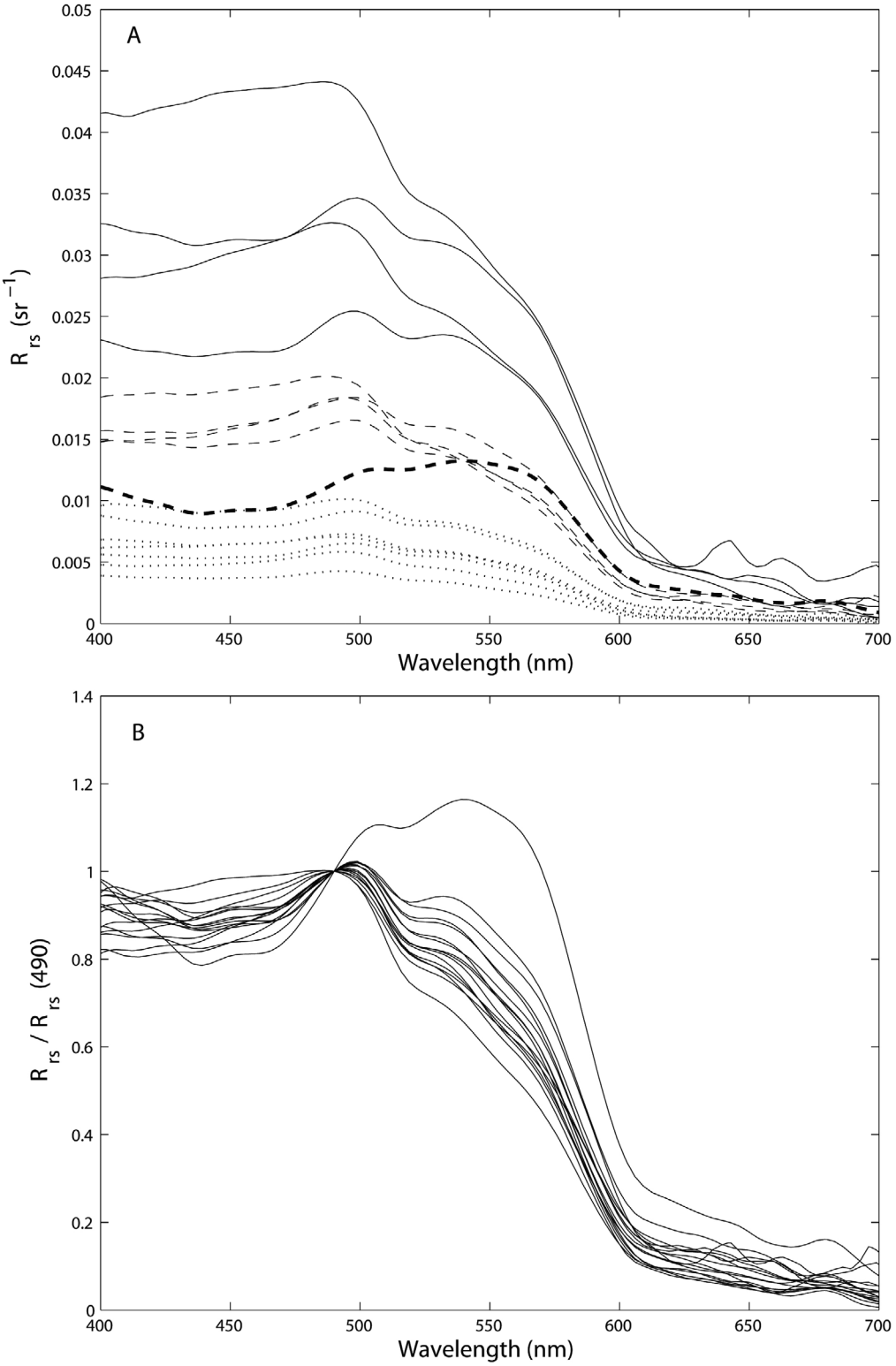

Figure 7. (a) Spectral remote sensing reflectance (R_{rs}, sr^{-1}) obtained from radiometric measurements at 16 stations sampled during the PATEX 5 cruise. Solid lines correspond to spectra at stations located within the highly reflective patch, dashed lines correspond to intermediate locations, and dotted lines correspond to stations located outside the patch (see text for station numbers). The dashed/bold line corresponds to the distinct spectra found at St. P512, where dominance of diatoms was found. (b) R_{rs} spectra normalized at 490 nm.

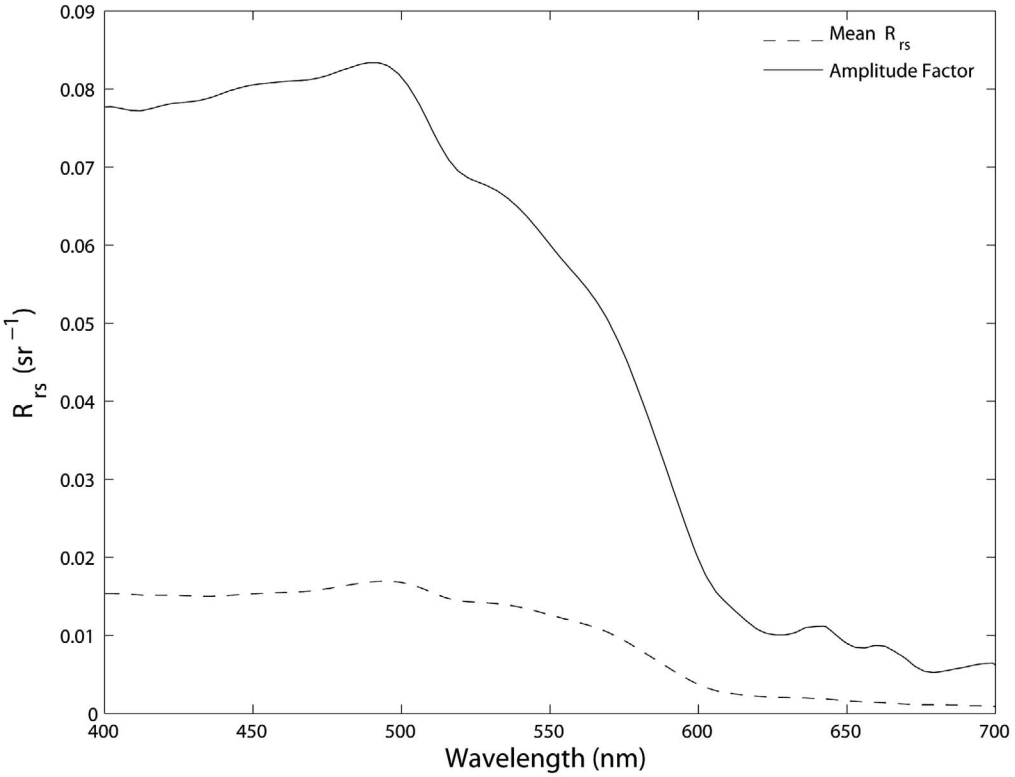

Figure 8. The mean R_{rs} spectra from all the sampled stations during PATEX 5 (N = 16) and the first dominant mode spectra which explains 98% of the total $R_{rs}(\lambda)$ variance.

able. Maximum concentrations were found at the stations located well within the center of the bloom (St. P514, PIC ~300 μg C L^{-1} and POC ~200 μg C L^{-1}), while the minimum concentrations were found at the stations located outside the high-reflective patch (e.g., St. P501, PIC ~35 μg C L^{-1} and POC ~326 μg C L^{-1}). The PIC range was relatively wide, with a mean value of 122 and a CV = 70%, while POC presented a lower variability, a mean value of 303 μg C L^{-1} and CV = 19%. PIC:POC ratio was highly variable (ranging between 0.02 and 1.1), mainly due to high PIC variability. This ratio showed a significant correlation with $b_{bp}(660)$ (r = 0.83, N = 10, $p < 0.005$). Furthermore, no significant correlation was found between POC and PIC, or between b_{bp}, c_p and a_p versus POC, while a strong correlation was found between PIC and b_{bp} (r = 0.81, N = 10, $p < 0.005$), and PIC and c_p (r = 0.7, N = 10, $p < 0.05$). This indicates that particulate scattering properties (b_{bp}, c_p) are mainly controlled by PIC while particulate absorption properties by phytoplankton (see section 3.3). A weak correlation between [*chl*] and POC (r = 0.56, N = 10, p = 0.07) as well as a lack of correlation between POC and absorption properties were found in this work. Table 2 summarizes the statistical relationships between bio-optical data and biogeochemical parameters.

3.7. Hyperspectral Remote Sensing Reflectance

[35] The absolute hyperspectral remote sensing reflectance R_{rs} spectra measured at 16 of the 18 stations sampled during the PATEX 5 cruise are shown in Figure 7a. A variability of approximately ten fold was observed at lower wavelengths, but a general flattened shape and high values at the blue portion of the spectrum (400–450 nm) compared to higher wavelengths, as well as a peak centered around 490 nm, can be observed in most spectra. Stations located within the high-reflective patch observed in the MODIS-derived normalized water leaving radiance at 551 nm (see Figure 1) are characterized by the highest reflectance in the entire spectral range (solid curves in Figure 7a corresponding to stations P503, P504, P514 and P515), while stations located outside the visible patch are characterized by the lowest reflectance (dotted curves in Figure 7a corresponding to P501, P508, P509, P510, P516, P517 and P518). Stations located relatively close to the bright feature present intermediate values (dashed curves in Figure 7a corresponding to P502, P507, P511 and P513).

[36] Figure 7b shows the normalized spectra at 490 nm, where a different spectral shape is apparent at station P512, showing a reflectance maximum at 540 nm. This distinctive shape was associated with dominance of diatoms (>50% biovolume). In general, some variability was also observed in the blue (~450 nm) and green (550 nm) parts of the spectrum.

[37] A Principal Component Analysis applied to the hyperspectral R_{rs} data set has shown that the first mode (Figure 8) accounted for 98% of the total R_{rs} variance. Not surprisingly, this spectral shape resembled the mean R_{rs} spectra. Correlation coefficients between the amplitude factors of the first mode and different bio-optical properties

Table 3. Correlation Coefficient Calculated Between the PCA First Amplitude Factor and in Situ Bio-optical Parameters ($p < 0.05$)[a]

Bio-optical Parameters	r	N
$b_{bp}(660)$	0.93	16
b_{bp}:$b_p(660)$	0.83	16
$a_p(440)$	NS	16
[*chl*]	NS	16
PIC	0.77	10
POC	NS	10
% *EH* cells	0.86	16
Coccolithophorid abundance (microscopy)	0.59	16

[a]NS, not significant.

were calculated (Table 3). The highest significant correlation was found for the particulate backscattering coefficient and backscattering ratio at 660 nm (r = 0.93 and 0.83, respectively). Conversely, no significant correlation was found between [*chl*], $a_p(440)$ or POC, indicating a dominance of the backscattering mechanism in controlling the reflectance variability in the sampled waters regardless their absorption properties. A poor though significant correlation ($r \sim 0.6$) was found between the first PCA mode and the coccolithophorid cell concentration (Table 3) as determined by microscopy [*Souza et al.*, 2011]. However, the first PCA mode correlates well with both PIC (r = 0.77, N = 10, $p < 0.05$) and % *EH* cells (r = 0.86, N = 16, $p < 0.05$), clearly an indication that most of R_{rs} spectral variability is associated with the relative presence of coccolithophorid in relation to other phytoplankton groups.

3.8. Performances of Chlorophyll and PIC Concentration Algorithms

[38] The performances of remote sensing algorithms for retrieving [*chl*] and PIC concentrations using in situ radiometric measurements were analyzed. NASA's SeaWiFS and MODIS operational algorithms (OC4v4 and OC3M, respectively), based on blue-to-green ratios, were analyzed using measured remote sensing reflectance and in situ surface [*chl*] determined by HPLC analysis. Similar results were found for both algorithms, thus only results corresponding to OC4v4 are shown in Figure 9a. Even though the measurements fell within the "cloud" of data comprising the global data set used for NASA's operational algorithms generation (gray crosses in Figure 9a), both algorithms tended to overestimate in situ measurements. Therefore, a poor performance was found between satellite-derived and in situ [*chl*] estimates for both OC4v4 (relative percent difference, *RPD* = 80%) and OC3M (*RPD* = 84%) algorithms. The errors found in this study are higher than others previously found in this area [*Garcia et al.*, 2005; *Dogliotti et al.*, 2009], but comparable to the errors found for coastal regions influenced by continental discharge from La Plata River and Patos Lagoon [*Garcia et al.*, 2006].

[39] We applied the two-band algorithm to estimate PIC concentration [*Balch et al.*, 2005] to the in situ normalized water-leaving radiances as implemented in SeaDAS (SeaWiFS Data Analysis System, version 6.1). The algorithm root-mean-square (RMS) error in PIC determination was high, 97.9 μg PIC L^{-1}, compared to the overall RMS error of 28 μg PIC L^{-1} found for the original algorithm [*Balch et al.*, 2005]. The two-band algorithm uses as input the

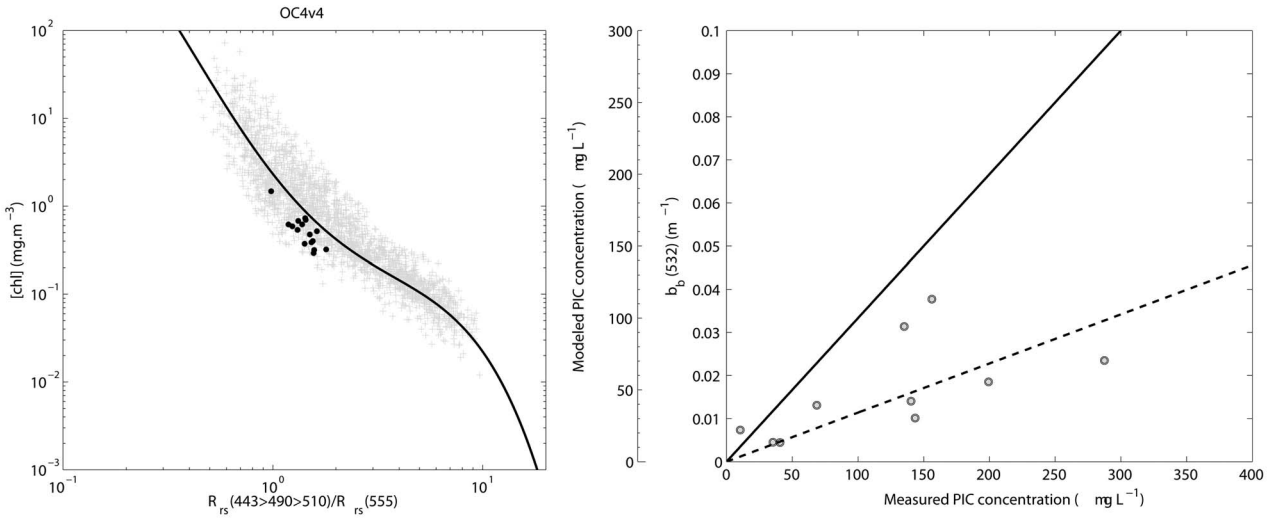

Figure 9. (a) Relationship between maximum blue-green bands ratio and chlorophyll concentration. NOMAD (gray crosses) and PATEX 5 (black circles) bio-optical data are displayed on figure (N = 16). The OC4v4 [*O'Reilly et al.*, 2000] chlorophyll algorithm is also shown (solid curve). (b) Modeled PIC concentration using the two-band algorithm [*Balch et al.*, 2005] versus measured values. As in the work of *Balch et al.* [2005], a second y axis was added showing the intermediate backscattering (b_b) value obtained from the LUT. The slope of the solid line is the current specific backscattering coefficient in use (3.33×10^{-4} m^2 mg PIC^{-1}), and the slope of the dashed line is the former value (1.14×10^{-4} m^2 mg PIC^{-1}) assumed by *Balch et al.* [2005].

normalized-water leaving radiance values at 443 and 547 nm in order to get the backscattering coefficient at 547 nm. The computation is performed from a LUT previously obtained by inversion of a semianalytical model [*Gordon et al.*, 1988]. Finally, PIC concentration is retrieved from the backscattering coefficient using a mean PIC-specific coefficient (i.e., backscattering coefficient normalized by PIC concentration), provided by *Balch et al.* [2005]. The original value used by *Balch et al.* [2005] for this coefficient was 1.14×10^{-4} m^2 mg PIC^{-1}, while current value in use is 3.33×10^{-4} m^2 mg PIC^{-1}, which was obtained by fitting a larger in situ database of PIC and b_b. Our in situ data showed a lower RMS error (81.5 μg PIC L^{-1}) and a slope closer to 1 (equations in Figure 9) when the original PIC-specific backscattering was used (dashed line in Figure 9b). Moreover, a good correlation was found between measured PIC and b_b values, whose equation describing the best least square linear fit is $b_b = 1.07 \times 10^{-4} \times \mathrm{PIC} + 0.005$, $r^2 = 0.63$, $N = 10$, $p < 0.005$.

4. Discussion

[40] Previous satellite image analyses have suggested the occurrence of coccolithophorid blooms in the Patagonian Region [*Brown and Yoder*, 1994; *Brown and Podestá*, 1997]. More recently, *Signorini et al.* [2006] assessed the timing and duration of coccolithophorid blooms along the Patagonian shelf-break, as well as the mechanisms that drive and maintain these blooms, using time series from satellite images and hydrographic data. Although remote sensing studies in the past have shown the presence of coccolithophorid blooms in this region, to our knowledge, this is the first report of a coccolithophorid bloom and associated apparent and inherent optical properties in Patagonian shelf waters.

[41] The key environmental and ecological factors controlling the blooms of these organisms are particularly: light, mixed layer depth, coupled with photoadaptation [see *Tyrrell and Merico*, 2004]. According to their review, the presence of coccolithophorids in surface waters are associated with highly stratified waters and mixed layers almost always shallower than 30 m. The physical structure of the water column in the present study met the adequate conditions for occurrence of these blooms, with a strong seasonal thermocline (Figure 2b), which probably prevented nutrients supply to the surface layer, during that period.

[42] The lack of covariation between dissolved oxygen and chlorophyll suggests that physical processes are probably controlling the gas levels. The potentially significant biological control of gases such as O_2 and CO_2 at surface layers of the Patagonian region are well known in situations of relatively high chlorophyll values [*Bianchi et al.*, 2009] and primary production rates associated to diatom dominance [*Garcia et al.*, 2008]. This would be the opposite under dominance of other groups and lower phytoplankton biomass [*Schloss et al.*, 2007]. A relatively low [*chl*] was observed associated to the coccolithophorid bloom found in this cruise, as compared to high concentrations measured in other bloom periods in the Patagonian shelf [*Carreto et al.*, 1995; *Papparazzo et al.*, 2010] and shelf-break [*Garcia et al.*, 2008; *Ferreira et al.*, 2009]. However, even at lower biomass levels, organisms with calcium carbonate shells are known to modify CO_2 levels in the water column [*Zondervan*, 2007], supporting the idea that the biological role in controlling gas concentration levels in the Patagonian region depends on the time of the year and the phytoplankton community.

[43] The sampled waters were visually characterized by the occurrence of a milky turquoise color caused by increased scattering properties, attributed to coccolithophorid cells as well as to their detached coccoliths. As already mentioned in section 2, the time evolution of satellite images (*nLw551*) suggests that the cruise timing corresponded to an advanced stage of the coccolithophorid bloom. In addition, the relatively high PIC:POC ratios and the significant relationship between PIC and particulate backscattering coefficient at 660 nm ($r = 0.83$) indicate that calcite platelets comprised a major portion of particle backscattering at the region. Both satellite and in situ measurements showed a high spatial variability of reflectances, with higher values found at the center of the patch than at the boundaries (Figure 1), probably indicating different growth stages of the bloom. High backscattering ratios found at all stations are also an indication of the declining phase of the bloom. It is worth noting that the highest values were found in those stations located closer to the bloom center. Current knowledge suggests that high b_{bp}:b_p values are generally observed in the presence of relatively high concentrations of inorganic particles, with high refractive index [*Loisel et al.*, 2007]. The values reported here are similar to values found in previous studies carried out in different coastal environments [*Boss et al.*, 2004; *Loisel et al.*, 2007; *Twardowski et al.*, 2001] and to the ones described by *Bricaud and Morel* [1986] for detached coccoliths, which are 2 orders of magnitude greater than those from intact cells. The sampled stations were located far from land where the influence of sediment resuspension is highly improbable. Our measurements of $b_{bp}(532)$ and $b_{bp}(660)$ have shown a $\lambda^{-0.16}$ dependence (see Figure 6), which means that b_{bp} increases slightly from the green to red portion of the visible spectrum, in agreement with b_{bp} patterns observed by *Gordon et al.* [2009]. The estimated backscattering probability in our work is also very close to the values modeled by *Gordon et al.* [2009].

[44] Even though coccolithophorids were present at the sampled stations, the bio-optical properties measured within this highly scattering patch showed a large spatial variability. The particulate backscattering and attenuation coefficients presented a similar spatial distribution that generally differed from that of chlorophyll concentration (Figure 5). The b_{bp} and c_p maxima, found at stations P503, P504, P514 and P515, were generally associated with relatively low [*chl*]. An exception was station P512 (Section 2), where their maxima corresponded with the highest [*chl*] found in the whole cruise. That station showed a different remote sensing spectral shape compared to the remaining stations (Figures 7a and 7b), showing a peak at 540 nm and lower R_{rs} values around 440 nm (chlorophyll maximum absorption region). Probably, the distinctive spectrum found was mainly associated with the phytoplankton community composition. That station was dominated by diatoms, but also influenced by the presence of coccolithophorids, thus the optical properties of both groups influenced the shape and magnitude of the R_{rs} spectra.

[45] In general, the $R_{rs}(\lambda)$ spectra found in this study (Figure 7a) showed similar shapes to the SeaWiFS-derived R_{rs} spectra shown by *Siegel et al.* [2007, Figure 5]. Even

when their values are limited to discrete wavelengths, they also found, at stations influenced by the presence of coccolithophorids, a flat shape and high reflectance values in the blue bands (412 and 443 nm), a peak at 490 nm, as well as a shift in this peak to 550 nm band where diatoms and dinoflagellates dominated. Moreover, our absolute reflectance values are comparable to the ones found in their work.

[46] The fundamental role of the backscattering coefficients in determining the reflectance hyperspectral properties of the coccolithophorid bloom, regardless the absorption properties, is confirmed by the strong relation between the first mode (which explains almost the total variance of the data set) of the PCA and b_{bp} and b_{bp}:b_b coefficients. Note that there was a lack of correlation between scattering or backscattering and absorption coefficients, indicating that different compartments control absorption and scattering properties in the presence of a coccolithophorid bloom. Living cells ([*chl*]) mainly control absorption while PIC dominates the scattering properties. Both the concentration as well as the composition of the inorganic material (through b_{bp} and b_{bp}:b_p, respectively) and the percentage of *E. huxleyi* cells, i.e., their proportion to other phytoplankton groups, explained most of the R_{rs} variability. Moreover, a good correlation (r = 0.93) was found between $b_{bp}(532)$ and $R_{rs}(532)$ (Table 2). On the other hand, the low correlation found between *E. huxleyi* cell concentration and both the PCA first mode ($r \sim 0.6$) and the $b_{bp}(532)$ ($r = 0.47$) suggests that the presence of high coccoliths:cell ratios (not taken into account by either of the mentioned methodologies) are responsible for the high R_{rs} values observed as has been previously suggested [*Holligan et al.*, 1983; *Bricaud and Morel*, 1986; *Balch et al.*, 1996a]. The lack of correlation between scattering (or backscattering) and absorption coefficients (or POC) may also indicate the dominance of detached coccoliths. Unfortunately, there are no data on detached coccolith numbers, so we were unable to explore directly their influence on the bio-optical parameters. Note that no significant relationship was evident between the first mode and absorption properties. Similarly, *Lubac and Loisel* [2007] applied Principal Component Analysis on a large R_{rs} hyperspectral data set with a relatively large variability. Interestingly, they found that the second mode of variability was explained by [*chl*], as well as the dissolved compartment absorption. In fact, this was also found in R_{rs} data analysis for other cruises in the Patagonian shelf-break region, with distinct community phytoplankton structures (A. Ferreira, Bio-optical characteristics of the Patagonian shelf-break waters: Implications for ocean color algorithms, manuscript in preparation, 2011).

[47] Light scattering from high concentrations of particulate material, such as the particulate calcite commonly found in coccolithophorid blooms (particularly *E. huxleyi*), is known to introduce errors in the estimation of chlorophyll concentration when band ratio algorithms are applied [*Gordon et al.*, 1988; *Balch et al.*, 1989; *Ackleson et al.*, 1994]. *Gordon et al.*'s [1988] semianalytical model predicted that in a coccolithophorid bloom chlorophyll concentration would be overestimated at low pigment concentration (<0.3 mg m^{-3}), if the coccoliths contribution was ignored, and it would be underestimated at high concentrations. Moreover, *Ackleson et al.* [1994] obtained similar results using a coupled atmosphere and ocean radiative transfer model developed to simulate water-leaving radiance from a vertically stratified ocean containing a bloom of *E. huxleyi*. Their differences were for concentrations lower and higher than 0.8 mg m^{-3}. Thus the overestimation we observed in this study is in accordance with the general tendency, but our results are closer to *Ackleson et al.*'s [1994] model's prediction since almost all the chlorophyll concentrations measured were below 0.8 mg m^{-3}, except for St. P512 (1.48 mg m^{-3}), where the empirical algorithms also overestimated the measured values. The general overestimation of [*chl*] derived from ocean color during coccolithophorid blooms has been mainly attributed to high backscattering coefficients induced by detached coccoliths [*Balch et al.*, 1996b]. Given that this information is not available in the present study, we analyzed and compared the chlorophyll-specific particulate backscattering coefficient at 532 nm (b_{bp}/[*chl*]) to an average value [*Loisel et al.*, 2010] and we found relatively high and variable values, with a mean of 0.0322 mg^{-1} m^2 and CV = 103.6%. In fact, most of the stations showed values higher than 0.009 mg^{-1} m^2, threshold used by *Loisel et al.* [2010] to classify waters as very turbid. Thus the overestimation of the blue-to-green algorithms found in this study is mainly due to high values of b_{bp}/[*chl*], i.e., higher than average values found in Case 1 waters.

[48] The 2-band PIC algorithm tested using the current specific backscattering coefficient generally showed a tendency to underestimate in situ values with a high RMS error (Figure 9b). However, if the original coefficient is used, the RMS error in PIC determination is greatly reduced. Moreover, this original b^*_{bPIC} is similar to the slope of the linear regression found in this study using the in situ values. This corroborates the existence of some variability in the PIC-specific backscattering, which can be attributed to changes in size and/or shape of the particles [*Balch et al.*, 1999]. Thus if the original PIC-specific backscattering coefficient is used in the algorithm, better estimates of PIC concentrations are retrieved, though some scatter in the data still exists. Possible errors associated with both measurements should be considered. Moreover, relatively few data points were available for the analysis (N = 10) and thus more bio-optical data could probably help improving algorithms to estimate PIC concentration using satellite images in this region.

5. Summary and Conclusions

[49] In the first week of January 2008, a cruise was conducted in highly reflective waters on the Argentinean continental shelf. The physical environmental conditions found during the cruise are in accordance to the adequate conditions for occurrence of these blooms, i.e., shallow mixed layer and strong stratification. A conspicuous bloom of coccolithophorids (mainly *Emilliania huxleyi*) was found and verified by miscroscopic analyses. Both satellite-derived *nLw551* time series imagery and in situ bio-optical measurements, combined with high PIC:POC values suggested an advanced stage of the sampled coccolithophorid bloom, with high coccolith:cell ratios. These small inorganic platelets are very effective scatters, particularly when detached from the cells in late stages of the bloom. In fact, backscattering was the main property influencing R_{rs} variability.

[50] This comprehensive field experiment confirmed that the highly reflective patches, usually detected by visible satellite images in this region, corresponded to a coccolithophorid bloom and that the remote sensing of chlorophyll using global algorithms in these blooms can be biased. In addition, a general satellite PIC algorithm was applied for the first time in this region to a set of in situ radiometric data. A poor performance was observed but better results were obtained when a previous PIC-specific backscattering coefficient was used, evidencing the need for more in situ bio-optical measurements for a better tuning of the PIC algorithm. Improved PIC estimates in this region, where large coccolithophorid blooms are known to occur, will contribute to further studies about their impact on the carbon cycle and their influence on the Earth's climate system.

Notation

Symbol	Definition	Unit
λ	Wavelength	nm
a_p	Particle absorption coefficient	m^{-1}
a_{det}	Detritus absorption coefficient	m^{-1}
a_{ph}	Phytoplankton absorption coefficient	m^{-1}
a_{CDOM}	Colored dissolved organic matter absorption coefficient	m^{-1}
a^*_{ph}	Specific phytoplankton absorption coefficient	m^2 mg $[chl]^{-1}$
b_{bp}	Particulate backscattering coefficient	m^{-1}
b_p	Particulate scattering coefficient	m^{-1}
b_{bp}:b_p	Particulate backscattering ratio	
b_{bp}:[chl]	Chlorophyll-specific particulate backscattering coefficient	mg^{-1} m^2
c_p	Particulate beam attenuation coefficient	m^{-1}
R_{rs}	Remote sensing reflectance	sr^{-1}
E_d	Downwelling irradiance	W m^2
L_u	Upwelling radiance	W m^2 sr^{-1}
nLw	Normalized water-leaving radiance	W m^2 sr^{-1}
K_d	Diffuse attenuation coefficient of downwelling irradiance	m^{-1}
K_L	Diffuse attenuation coefficient of upwelling radiance	m^{-1}
[chl]	Chlorophyll-a concentration	mg m^{-3}
PIC	Particulate inorganic carbon concentration	μg PIC L^{-1}
POC	Particulate organic carbon concentration	μg POC L^{-1}
% *EH* cells	Cell percentage of *Emiliania huxleyi*	%

[51] **Acknowledgments.** The Patagonian Experiment (PATEX) is a multidisciplinary project part of the Group of High Latitude Oceanography (GOAL) activities in the Brazilian Antarctic Program. We thank the crew of the Brazilian Navy RV *Ary Rongel* for their assistance during the field sampling. We also acknowledge the Servicio de Hidrografia Naval (Argentina) for their cooperation in obtaining clearance for carrying out field work within Argentinean EEZ. We thank Michael Novak at NASA/GSFC for analyzing the POC and PIC samples. The cruise PATEX 5 was conducted under the umbrella of the project "Southern Ocean Studies for Understanding Climate Changes Issues" (SOS-CLIMATE), a Brazilian contribution to the International Polar Year. We would like to thank two anonymous reviewers whose criticisms and suggestions have improved this manuscript. The project was sponsored through the funding resources of Ministry of Science and Technology (MCT) and CNPq (Brazilian National Council on Research and Development, grant 520189/2006–0) to the Brazilian Antarctic Program (PROANTAR). This work was partly supported by GSFC/NASA through the project OCEANS/04123400362. Ocean color images were provided by and processed at the Goddard Space Flight Center (GSFC).

References

Ackleson, S., W. M. Balch, and P. M. Holligan (1994), Response of water-leaving radiance to particulate calcite and chlorophyll a concentrations: A model for Gulf of Maine coccolithophore blooms, *J. Geophys. Res.*, *99*, 7483–7499, doi:10.1029/93JC02150.

Austin, R. W. (1974), The remote sensing of spectral radiance from below the ocean surface, in *Optical Aspects of Oceanography*, edited by N. G. Jerlov and E. S. Nielsen, pp. 317–344, Academic Press, London.

Balch, W. M., R. W. Eppley, M. R. Abbott, and F. M. H. Reid (1989), Bias in satellite-derived pigment measurements due to coccolithophores and dinoflagellates, *J. Plankton Res.*, *11*, 575–581, doi:10.1093/plankt/11.3.575.

Balch, W. M., P. M. Holligan, S. Ackleson, and K. Voss (1991), Biological and optical properties of mesoscale coccolithophore blooms in the Gulf of Maine, *Limnol. Oceanogr.*, *36*, 629–643, doi:10.4319/lo.1991.36.4.0629.

Balch, W. M., K. A. Kilpatrick, P. M. Holligan, and C. Trees (1996a), The 1991 coccolithophore bloom in the central North Atlantic: I. Optical properties and factors affecting their distribution, *Limnol. Oceanogr.*, *41*, 1669–1683, doi:10.4319/lo.1996.41.8.1669.

Balch, W. M., K. A. Kilpatrick, P. M. Holligan, D. Harbour, and E. Fernandez (1996b), The 1991 coccolithophore bloom in the central North Atlantic. II. Relating optics to coccolith concentration, *Limnol. Oceanogr.*, *41*, 1684–1696, doi:10.4319/lo.1996.41.8.1684.

Balch, W. M., D. T. Drapeau, T. L. Cucci, R. D. Vaillancourt, K. A. Kilpatrick, and J. J. Fritz (1999), Optical backscattering by calcifying algae—Separating the contribution by particulate inorganic and organic carbon fractions. *J. Geophys. Res.*, *104*, 1541–1558.

Balch, W. M., D. T. Drapeau, B. Bowler, and J. Fritz (2000), Continuous measurements of calcite-dependent light scattering in the Arabian Sea, *Deep Sea Res., Part I*, *48*, 2423–2452.

Balch, W. M., H. R. Gordon, B. C. Bowler, D. T. Drapeau, and E. S. Booth (2005), Calcium carbonate budgets in the surface global ocean based on moderate-resolution imaging spectroradiometer data, *J. Geophys. Res.*, *110*, C07001, doi:10.1029/2004JC002560.

Bianchi, A. A., D. Ruiz-Pino, H. Isbert Perlender, A. P. Osiroff, V. Segura, V. A. Lutz, M. Luz Clara, C. F. Balestrini, and A. R. Piola (2009), Annual balance and seasonal variability of sea-air CO_2 fluxes in the Patagonia Sea: Their relationship with fronts and chlorophyll distribution, *J. Geophys. Res.*, *114*, C03018, doi:10.1029/2008JC004854.

Boeckel, B., K. H. Baumann, R. Henrich, and H. Kinkel (2006), Coccolith distribution patterns in South Atlantic and Southern Ocean surface sediments in relation to environmental gradients, *Deep Sea Res., Part I*, *53*, 1073–1099, doi:10.1016/j.dsr.2005.11.006.

Boss, E., and W. S. Pegau (2001), Relationship of light scattering at an angle in the backward direction to the backscattering coefficient, *Appl. Opt.*, *40*, 5503–5507, doi:10.1364/AO.40.005503.

Boss, E., W. S. Pegau, M. Lee, M. Twardowski, E. Shybanov, G. Korotaev, and F. Baratange (2004), Particulate backscattering ratio at LEO 15 and its use to study particle composition and distribution, *J. Geophys. Res.*, *109*, C01014, doi:10.1029/2002JC001514.

Bricaud, A., and A. Morel (1986), Light attenuation and scattering by phytoplanktonic cells: A theoretical modeling, *Appl. Opt.*, *25*, 571–580, doi:10.1364/AO.25.000571.

Bricaud, A., M. Babin, A. Morel, and E. H. Claustre (1995), Variability in the chlorophyll specific absorption coefficients of natural phytoplankton: Analysis and parameterization, *J. Geophys. Res.*, *100*(C7), 13,321–13,332.

Bricaud, A., H. Claustre, J. Ras, and K. Oubelkheir (2004), Natural variability of phytoplanktonic absorption in oceanic waters: Influence of the size structure of algal populations, *J. Geophys. Res.*, *109*, C11010, doi:10.1029/2004JC002419.

Brown, C. W., and G. P. Podestá (1997), Remote sensing of coccolithophore blooms in the western South Atlantic Ocean, *Remote Sens. Environ.*, *60*(1), 83–91, doi:10.1016/S0034-4257(96)00140-X.

Brown, C. W., and J. A. Yoder (1994), Coccolithophorid blooms in the global ocean, *J. Geophys. Res.*, *99*, 7467–7482, doi:10.1029/93JC02156.

Carreto, J. I., V. A. Lutz, M. O. Carignan, A. D. C. Colleoni, and S. G. D. Marcos (1995), Hydrography and chlorophyll-a in a transect from the coast to the shelf-break in the Argentinean Sea, *Cont. Shelf Res.*, *15*, 315–336, doi:10.1016/0278-4343(94)E0001-3.

Chang, G. C., T. Dickey, C. Moore, A. Barnard, R. Zaneveld, A. Hanson, and P. Egli (2004), Bio-optical relationships in the Santa Barbara Channel: Implications for remote sensing, paper presented at the Ocean Optics XVII Conference, Fremental, Australia, 25–29 October.

Dogliotti, A. I., I. R. Schloss, G. O. Almanedoz, and D. A. Gagliardini (2009), Evaluation of SeaWiFS and MODIS chlorophyll-a products in the Argentinean Patagonian continental shelf (38°S–55°S), *Int. J. Remote Sens.*, *30*, 251–273, doi:10.1080/01431160802311133.

Ferreira, A., V.M.T. Garcia, and C. A. E. Garcia (2009), Light absorption by phytoplankton non-algal particles and dissolved organic matter at the Patagonia shelf-break in spring and summer, *Deep Sea Res. Part I*, doi:10.1016/j.dsr.2009.08.002.

Garcia, C. A. E., Y. V. B. Sarma, M. M. Mata, and V. M. T. Garcia (2004), Chlorophyll variability and eddies in the Brazil-Malvinas confluence region, *Deep Sea Res., Part II*, *51*(1–3), 159–172, doi:10.1016/j.dsr2.2003.07.016.

Garcia, C. A. E., V. M. T. Garcia, and C. R. McClain (2005), Evaluation of SeaWiFS chlorophyll algorithms in the southwestern Atlantic and Southern oceans, *Remote Sens. Environ.*, *95*, 125–137, doi:10.1016/j.rse.2004.12.006.

Garcia, V. M. T., S. Signorini, C. A. E. Garcia, and C. R. McClain (2006), Empirical and semi-analytical chlorophyll algorithms in the southwestern Atlantic coastal region (25-40°S and 60–45°W), *Int. J. Remote Sens.*, *27*(8), 1539–1562, doi:10.1080/01431160500382857.

Garcia, V. M. T., C. A. E. Garcia, M. M. Mata, R. C. Pollery, A. R. Piola, S. R. Signorini, C. R. McClain, and M. D. Iglesias-Rodríguez (2008), Environmental factors controlling the phytoplankton blooms at the Patagonia shelf-break in spring, *Deep Sea Res., Part I*, *55*(9), 1150–1166, doi:10.1016/j.dsr.2008.04.011.

Garver, S. A., and D. A. Siegel (1997), Inherent optical property inversion of ocean color spectra and its biogeochemical interpretation: 1. Time series from the Sargasso Sea, *J. Geophys. Res.*, *102*, 18,607–18,625.

Gonzalez-Silvera, A., E. Santamaria-del-Angel, V. M. T. Garcia, C. A. E. Garcia, R. Millan-Nunez, and F. Muller-Karger (2004), Biogeographical regions of the tropical and subtropical Atlantic Ocean off South America: Classification based on pigment (CZCS) and chlorophyll-a (SeaWiFS) variability, *Cont. Shelf Res.*, *24*, 983–1000, doi:10.1016/j.csr.2004.03.002.

Gordon, H. R., and W. M. Balch (1999), MODIS Detached Coccolith Concentration Algorithm Theoretical Basis Document, Version 4, Algorithm Theoretical Basis Document. (Available at http://modis.gsfc.nasa.gov/data/atbd/atbd_mod23.pdf)

Gordon, H. R., and T. Du (2001), Light scattering by nonspherical particles: Application to coccoliths detached from *Emiliania huxleyi*, *Limnol. Oceanogr.*, *46*, 1438–1454, doi:10.4319/lo.2001.46.6.1438.

Gordon, H. R., O. B. Brown, R. H. Evans, J. W. Brown, R. C. Smith, K. S. Baker, and D. K. Clark (1988), A semianalytic radiance model of ocean color, *J. Geophys. Res.*, *93*, 10,909–10,924, doi:10.1029/JD093iD09p10909.

Gordon, H. R., G. C. Boynton, W. M. Balch, S. B. Groom, D. S. Harbour, and T. J. Smyth (2001), Retrieval of coccolithophore calcite concentration from SeaWiFS imagery, *Geophys. Res. Lett.*, *28*, 1587–1590, doi:10.1029/2000GL012025.

Gordon, H. R., T. J. Smyth, W. M. Balch, G. C. Boynton, and G. A. Tarran (2009), Light scattering by coccoliths detached from *Emiliania huxleyi*, *Appl. Opt.*, *48*, 6059–6073, doi:10.1364/AO.48.006059.

Hedges, J. I., and J. H. Stern (1984), Carbon and nitrogen determinations of carbonate-containing solids, *Limnol. Oceanogr.*, *29*, 657–663, doi:10.4319/lo.1984.29.3.0657.

Hillebrand, H., C. D. Dürselen, D. Kirschtel, U. Pollingher, and T. Zohary (1999), Biovolume calculation for pelagic and benthic microalgae, *J. Phycol.*, *35*, 403–424, doi:10.1046/j.1529-8817.1999.3520403.x.

Holligan, P. M., M. Viollier, D. S. Harbour, P. Camus, and M. Champagne-Phillippe (1983), Satellite and ship studies of coccolithophore production along a continental shelf edge, *Nature*, *304*, 339–342, doi:10.1038/304339a0.

Holligan, P. M., S. B. Groom, and D. S. Harbour (1993), What controls the distribution of the coccolithophore, *Emiliania huxleyi*, in the North Sea?, *Fish. Oceanogr.*, *2*, 175–183, doi:10.1111/j.1365-2419.1993.tb00133.x.

Iglesias-Rodríguez, M. D., C. W. Brown, S. C. Doney, J. Kleypas, D. Kolber, Z. Kolber, P. K. Hayes, and P. G. Falkowski (2002), Representing key phytoplankton functional groups in ocean carbon cycle models: Coccolithophorids, *Global Biogeochem. Cycles*, *16*(4), 1100, doi:10.1029/2001GB001454.

Loisel, H., and A. Morel (1998), Light scattering and chlorophyll concentration in case 1 waters: A re-examination, *Limnol. Oceanogr.*, *43*, 847–857, doi:10.4319/lo.1998.43.5.0847.

Loisel, H., X. Mériaux, J. Berthon, and A. Poteau (2007), Investigation of the optical backscattering to scattering ratio of marine particles in relation to their biogeochemical composition in the eastern English Channel and southern North Sea, *Limnol. Oceanogr.*, *52*(2), 739–752, doi:10.4319/lo.2007.52.2.0739.

Loisel, H., B. Lubac, D. Dessailly, L. Duforêt-Gaurier, and V. Vantrepotte (2010), Effect of inherent optical properties variability on the chlorophyll retrieval from ocean color remote sensing: An in situ approach, *Opt. Express*, *18*(20), 20,949–20,959, doi:10.1364/OE.18.020949.

Lubac, B., and H. Loisel (2007), Variability and classification of remote sensing reflectance spectra in the eastern English Channel and southern North Sea, *Remote Sens. Environ.*, *110*(1), 45–58, doi:10.1016/j.rse.2007.02.012.

Mendes, C. R., P. Cataxana, and V. Brotas (2007), HPLC determination of phytoplankton and microphytobenthos pigments: Comparing resolution and sensitivity of a C_{18} and a C_8 method, *Limnol. Oceanogr. Methods*, *5*, 362–370.

Mitchell, G., et al. (2000), Determination of spectral absorption coefficients of particles, dissolved material and phytoplankton for discrete water samples, in *Ocean Optics Protocols for Satellite Ocean Color Sensor Validation, Revision 2*, edited by G. S. Fargion, J. L. Mueller, and C. R. McClain, pp. 125–153, NASA, Goddard Space Flight Cent., Greenbelt, Md.

Morel, A. (1974), Optical properties of pure water and pure seawater, in *Optical Aspects of Oceanography*, edited by N. G. Jerlov and E. Steeman Nielsen, pp. 1–24, Academic Press, New York.

Morel, A. (1988), Optical modeling of the upper ocean in relation to its biogenous matter content (case 1 water), *J. Geophys. Res.*, *93*, 10,749–10,768.

O'Reilly, J. E., et al. (2000), Ocean color chlorophyll-a algorithms for SeaWiFS, OC2 and OC4: Version 4, in *SeaWiFS Postlaunch Tech. Rep. Ser.*, *NASA/TM-2000–206892*, vol. 11, part 3, pp. 9–23, NASA Goddard Space Flight Cent., Greenbelt, Md.

Pak, H., D. A. Kiefer, and J. C. Kitchen (1988), Meridional variations in the concentration of chlorophyll and microparticles in the North Pacific Ocean, *Deep Sea Res., Part I.*, *35*, 1151–l171.

Papparazzo, F. E., L. Bianucci, I. R. Schloss, G. O. Almandoz, M. Solís, and J. L. Esteves (2010), Cross-frontal distribution of inorganic nutrients and chlorophyll-a on the Patagonian continental shelf of Argentina during summer and fall, *Rev. Biol. Mar. Oceanogr.*, *45*(1), 107–119.

Rivas, A. L., A. I. Dogliotti, and D. A. Gagliardini (2006), Seasonal variability in satellite-measured surface chlorophyll in the Patagonian shelf, *Cont. Shelf Res.*, *26*, 703–720.

Romero, S. I., A. R. Piola, M. Charo, and C. A. E. Garcia (2006), Chlorophyll-a variability off Patagonia based on SeaWiFS data, *J. Geophys. Res.*, *111*, C05021, doi:10.1029/2005JC003244.

Roesler, C. S., and M. J. Perry (1995), In situ phytoplankton absorption, fluorescence emission, and particulate backscattering spectra determined from reflectance, *J. Geophys. Res.*, *100*(C7), 13,279–13,294.

Roth, P. H., M. M. Mullin, and W. H. Berger (1975), Coccolith sedimentation by fecal pellets: Laboratory experiments and field observations, *Geol. Soc. Am. Bull.*, *86*, 1079–1084, doi:10.1130/0016-7606(1975)86<1079:CSBFPL>2.0.CO;2.

Schloss, I. R., G. A. Ferreyra, M. E. Ferrario, G. O. Almandoz, R. Codina, A. A. Bianchi, C. F. Balestrini, H. A. Ochoa, D. Ruiz-Pino, and A. Poisson (2007), Role of plankton communities in sea-air variations in pCO_2 in the SW Atlantic Ocean, *Mar. Ecol. Prog. Ser.*, *332*, 93–106, doi:10.3354/meps332093.

Siegel, H., T. Ohde, M. Gerth, G. Lavik, and T. Leipe (2007), Identification of coccolithophore blooms in the SE Atlantic Ocean off Namibia by satellites and in-situ methods, *Cont. Shelf Res.*, *27*, 258–274, doi:10.1016/j.csr.2006.10.003.

Signorini, S., V. M. T. Garcia, A. R. Piola, C. A. E. Garcia, M. M. Mata and C. R. McClain (2006), Seasonal and interannual variability of calcite in the vicinity of the Patagonian shelf break (38°S–52°S), *Geophys. Res. Lett.*, *33*, L16610, doi:10.1029/2006GL026592.

Sournia, A. (Ed.) (1978), *Phytoplankton Manual*, 337 pp., UNESCO, Mus. Natl. d'Hist. Nat., Paris.

Souza, M. S., et al. (2011), Phyto-plankton community during a Coccolithophorid bloom in the Patagonian shelf: Microscopic and HPLC pigment analyses, *J. Mar. Biol. Assoc. U. K.*, in press.

Twardowski, M. S., E. Boss, J. B. Macdonald, W. S. Pegau, A. H. Barnard, and J. R. Zaneveld (2001), A model for estimating bulk refractive index from the optical backscattering ratio and the implications for understanding particle composition in case I and case II waters, *J. Geophys. Res.*, *106*(C7), 14,129–14,142, doi:10.1029/2000JC000404.

Tyrrell, T., and A. Merico (2004), *Emiliania huxleyi*: Bloom observations and the conditions that induce them, in *Coccolithophores: From Molecular Processes to Global Impact*, edited by H. R. Thierstein and J. R. Young, pp. 75–97, Springer, Berlin.

Tyrrell, T., and A. H. Taylor (1995), Latitudinal and seasonal-variations in carbon-dioxide and oxygen in the northeast Atlantic and the effects on *Emiliania huxleyi* and other phytoplankton, *Global Biogeochem. Cycles*, *9*, 585–604, doi:10.1029/95GB01133.

Welschmeyer, N. A. (1994), Fluorometric analysis of chlorophyll-a in the presence of chlorophyll-b and pheopigments, *Limnol. Oceanogr.*, *39*(8), 1985–1992, doi:10.4319/lo.1994.39.8.1985.

Zondervan, I. (2007), The effects of light, macronutrients, trace metals and CO_2 on the production of calcium carbonate and organic carbon in coccolithophores: A review, *Deep Sea Res., Part II*, *54*, 521–537, doi:10.1016/j.dsr2.2006.12.004.

A. I. Dogliotti, IAFE-CONICET, Pab. IAFE-Ciudad Universitaria, C.C. 67- Suc. 28, 1428, Buenos Aires, Argentina.

A. Ferreira, C. A. E. Garcia, V. M. T. Garcia, M. M. Mata, and M. S. Souza, Instituto de Oceanografia, Universidade Federal do Rio Grande, 96201-900 Rio Grande, RS, Brazil. (dfsgar@furg.br)

S. I. Romero, Servicio de Hidrografía Naval, Av. Montes de Oca, 2124, 1271, Buenos Aires, Argentina.

A. Mannino, NASA Goddard Space Flight Center, Mail Code 614.2, Building 22, Room 250, Greenbelt, MD 20771, USA.